Supporting Information

Cooperative organic alloys nanoparticles built from matching pair of quadrupolar dyes showing unusual fluorescence behaviour

Eleonore Kurek,[a] Pietro Mancini,[b] Jean-Baptiste Verlhac,[a] Benedetta Carlotti,[*b] and Mireille Blanchard-Desce[*a]

[a] Université de Bordeaux, CNRS, Bordeaux INP, ISM (UMR5255), 351 Cours de la Libération, 33405 Talence, France.
* E-mail: mireille.blanchard-desce@u-bordeaux.fr

[b] Department of Chemistry, Biology and Biotechnology and CEMIN, University of Perugia, 06123 Perugia, Italy.
* E-mail: benedetta.carlotti@unipg.it

Table of Contents

I. Materials and Methods

1. Dye synthesis

Energy donor and acceptor PPDs D and A were prepared following a previously reported[1] synthetic route.

2. Nanoparticle preparation

Freshly distilled water and spectroscopic grade THF were used in the following. Stock solutions were prepared in THF from dyes A and D respectively, and then mixed to obtain various A/D concentration ratios, as indicated in the вFONs name. For example, вFONs(0.3/1) were prepared from a stock solution containing 0.3mM of A and 1mM of D. For single component AdFONs(1) and DdFONs(1), 1mM stock solutions of A or D were used. All вFONs and dFONs were prepared using the same nanoprecipitation protocol, by rapidly injecting the THF stock solution (200 µL) into distilled water (19.8 mL) under continuous 3-minute sonication at 10 W (1% final volume of THF in water). The nanoparticle suspensions were left to air out for 30 minutes to allow for THF evaporation and then centrifuged at 3000 rpm for 5 minutes, after which the supernatant was then collected.

3. Förster radius calculations

The Förster radius R_0 can be calculated for a single donor-acceptor pair using equation (1):

$$\mathbf{R_0^6} = (\mathbf{8.785} \times \mathbf{10^{-5}})\boldsymbol{\kappa}^{\mathbf{2}}\Phi \frac{\mathbf{J}}{\mathbf{n^4}} \qquad (1)$$

where κ is an orientation factor (here κ^2 = 0.476 was chosen to reflect random dipole orientations in the static regime[2]), Φ is the fluorescence quantum yield of the donor (Φ = 0.29), J is the overlap integral between donor emission and acceptor absorption (J = 1.1 $\times 10^{15}$ $M^{-1}.cm^{-1}.nm^4$) and n is the refractive index of the medium (n in FONs was assumed to be close to that of polystyrene n =1.59). Using equation (1), an $R_0^{D\text{-}A}$ value of 3.6 nm was obtained for a single D-A pair. Regarding homo-FRET between donors, $R_0^{D\text{-}D}$ was determined to be 1.9 nm, while for homo-FRET between acceptors, $R_0^{A\text{-}A}$ yielded 1.7 nm.

4. Morphological characterization

Transmission Electron Microscopy was performed on a Hitachi H7650 80 kV electron microscope. Copper grids coated with a polymer membrane were treated using the Glow discharge technique to yield a positively charged hydrophilic carbon surface to allow stronger interactions between the sample and the grid itself. One droplet of undiluted aqueous nanoparticle suspension was deposited on the grid for 1 minute, then the excess liquid was eliminated with paper. A staining procedure using uranyl acetate was then used to enhance the contrast. Size analysis was conducted on the resulting images using a Python segmentation analysis program (code available upon request and deposited on an online open access folder) to extract the nanoparticle diameters (Table S3).

Hydrodynamic diameters were determined by Dynamic Light Scattering (DLS) on a Zetasizer Nano SZ100Z Horiba instrument operating at 90°. Analysis was performed using the software supplied by the manufacturer, with a polydisperse and standard width size distribution as calculation settings. Diameters reported in Table S3 are the total mean values of intensity-based size distributions.

5. Photophysical studies

All photophysical studies were performed at room temperature in 1 cm quartz cuvettes, on freshly prepared air-equilibrated nanoparticle solutions at room temperature. Absorbance measurements were collected on a Jasco V-670 UV/Vis spectrophotometer. Fully corrected emission spectra were acquired using a FluoroMax spectrofluorometer, on diluted solutions with an absorbance maximum set to ≤ 0.1. Fluorescence quantum yields were measured according to literature procedures using standards Nile Blue in EtOH (Φ = 0.27) and 4-(dicyanomethylene)-2-methyl-6-[p-(dimethyl-amino) styryl]-4H-pyran in EtOH (Φ = 0.44) (see calculation details in the “вFONs brightness calculation” section). Fluorescence decays were measured in a time-correlated single photon counting (TCSPC) configuration, using an Edinburgh Instruments FLS1000 with a NanoLed-455 (Horiba) for excitation. The instrument response was determined by measuring the light scattered by an aqueous dispersion of Ludox (30% in water, Sigma–Aldrich). The lifetime values were obtained from the reconvolution fit analysis of the decay profiles; the quality of the fits was judged by the reduced χ^2 value. The reported lifetimes are within ±0.1 ns and are either amplitude (2) or intensity (3) averaged:

$$\boldsymbol{\tau}^{\boldsymbol{amp}} = \frac{\sum_i \boldsymbol{a_i \tau_i}}{\sum_i \boldsymbol{a_i}} \qquad (2)$$

$$\boldsymbol{\tau}^{\boldsymbol{int}} = \frac{\sum_i \boldsymbol{a_i \tau_i^2}}{\sum_i \boldsymbol{a_i \tau_i}} \qquad (3)$$

Where a_i are the normalized pre-exponential coefficients and τ_i are the individual fluorescence lifetimes.

6. BFONs brightness calculation

The theoretical brightness of BFONs upon donor excitation can be estimated using (4):

$$\boldsymbol{B = N\varepsilon_{BFONs}^{\lambda exc_D}\Phi} \qquad (4)$$

with $\boldsymbol{N}$ the average number of dyes per nanoparticle, calculated using : $N = \frac{4\pi\rho N_A}{3M}\left(\frac{\varnothing}{2}\right)^3$

with ρ the assumed density of the BFONs (1000 g/L),
M the average molar mass of a dye within BFONs ($M = \frac{[A]M(A)+[D]M(D)}{[A]+[D]}$, with $M(A)$ and $M(D)$ the molar masses of dye A and dye D, and $[A]$ and $[D]$ the introduced quantities of A and D),
$\varnothing$ the dry BFONs diameter (in dm),
N_A = 6.02×10^{23} mol^{-1}.

with $\boldsymbol{\varepsilon_{BFONs}^{\lambda exc_D}}$ the extinction coefficient of BFONs at the excitation wavelength of D, calculated as: $\varepsilon_{BFONs}^{\lambda exc_D} = \frac{A_{BFONs}^{\lambda exc_D}}{l(C_A+C_D)}$

where $A_{BFONs}^{\lambda exc_D}$ is the absorbance of fresh undiluted BFONs, at the excitation wavelength of the donor (445 nm), and C_A and C_D are the respective concentrations of A and D present in BFONs, which are experimentally determined using:

$$C_A = \frac{A_{BFONs}^{lyoph-THF}(580nm)}{\varepsilon_{THF}^{A}(580nm)l} \text{ and } C_D = \frac{A_{BFONs}^{lyoph-THF}(437nm) - C_A \times \varepsilon_{THF}^{A}(437nm)}{\varepsilon_{THF}^{D}(437nm)l}$$

where $\varepsilon_{THF}^{A}(580nm)$ is the molar extinction coefficient of A in THF at 580 nm (where D does not absorb),
$\varepsilon_{THF}^{D}(437nm)$ is the molar extinction coefficient of D in THF at 437 nm (where A absorbance is minimal),
$\varepsilon_{THF}^{A}(437nm)$ is the molar extinction coefficient of A in THF at 437 nm (used to remove the contribution from A absorbance when calculating C_D)
and $A_{BFONs}^{lyoph-THF}(\lambda)$ is obtained experimentally by freeze-drying a volume V of the undiluted BFONs suspension, resuspending the resulting solid in the same volume V of THF, and measuring the absorbance of this solution at 437 nm (D) and 580 nm (A), using cuvettes with l =1cm.

Such that the final expression of $\varepsilon_{BFONs}^{\lambda exc_D}$ is: $\varepsilon_{BFONs}^{\lambda exc_D} = \frac{A_{BFONs}^{\lambda exc_D} \times \varepsilon_{THF}^{A}(580nm) \times \varepsilon_{THF}^{D}(437nm)}{A_{BFONs}^{lyoph-THF}(580nm) \times \varepsilon_{THF}^{D}(437nm) + A_{BFONs}^{lyoph-THF}(437nm) \times \varepsilon_{THF}^{A}(580nm) - A_{BFONs}^{lyoph-THF}(580nm) \times \varepsilon_{THF}^{A}(437nm)}$

with $\boldsymbol{\Phi}$ the fluorescence quantum yield of BFONs upon donor excitation: $\Phi = \frac{n^2}{n_{\mathrm{ref}}^2} \times \frac{\int I_F}{\int I_{F\,\mathrm{ref}}} \times \left(\frac{1-10^{-A_{ref}}}{1-10^{-\mathrm{A}}}\right) \times \Phi_{\mathrm{ref}}$

where Φ_{ref} is the fluorescence quantum yield of the standard,
$\int I_F$ is the area under the curve of the emission spectrum of the sample excited at λ_{ex},
$\int I_{F\,ref}$ is the area under the curve of the emission spectrum of the reference excited at $\lambda_{ex\,ref}$,
A is the absorbance of the sample at λ_{ex},
A_{ref} is the absorbance of the reference at $\lambda_{ex\,ref}$,
n is the refractive index of the sample solvent,
n_{ref} is the refractive index of the reference solvent.

7. Probability calculations

The probability of encountering a particle containing n acceptors in an ensemble of BFONs containing $\overline{n_A}$ acceptors per particle on average can be described by the Poisson probability distribution function: $P(n, \overline{n_A}) = \frac{(\overline{n_A})^n}{n!e^{\overline{n_A}}}$

with:
n : the actual number of acceptors per nanoparticle.
$\overline{n_A}$: the average number of acceptors per nanoparticle (from preparation conditions): $\overline{n_A} = A_{\%}N$
with $A_{\%}$: the acceptor proportion contained in the BFONs: $A_{\%} = \frac{[A]}{[A]+[D]}$,with $[A]$ and $[D]$ the introduced quantities of A and D.
with N the total average number of dyes contained in a BFONs: $N = \frac{[A]+[D]}{[A]M(A)+[D]M(D)}\frac{4\pi\rho N_A}{3}\left(\frac{\varnothing}{2}\right)^3$

The probability of BFONs containing 0 acceptor molecules is thus: $P(n=0) = \frac{1}{e^{\overline{n_A}}}$ with $\overline{n_A} = \frac{[A]}{[A]+[D]}\frac{4\pi\rho N_A}{3M}\left(\frac{\varnothing}{2}\right)^3$, or:

$$\boldsymbol{P(n=0) = \exp\left(-\frac{[A]}{[A]+[D]}\frac{4\pi\rho N_A}{3M}\left(\frac{\varnothing}{2}\right)^3\right)} \qquad (5)$$

8. Ultrafast time-resolved measurements

The experimental setups for femtosecond transient absorption and broadband fluorescence up–conversion measurements have been widely described elsewhere.[3–5] In particular, the 400 nm excitation pulses of ca. 40 fs are generated by an amplified Ti:Sapphire laser system (Spectra Physics). The transient absorption set up (Helios, Ultrafast Systems) is characterized by temporal resolution of ca. 150 fs and spectral resolution of 1.5 nm. Probe pulses are produced in the 450–800 nm range by passing a small portion of 800 nm light through an optical delay line (with a time window of 3200 ps) and focusing it into a 2 mm thick Sapphire window to generate a white–light continuum. In the up–conversion set–up (Halcyone, Ultrafast Systems) the 400 nm pulses excite the sample whereas the remaining fundamental laser beam plays the role of the "optical gate" after passing through a delay line. The fluorescence of the sample is collected and focused onto a BBO crystal together with the delayed fundamental laser beam. A CCD detects the up–converted fluorescence. Movement of the crystal through a rotational stage allows for broadband detection of the emission at each delay and thus acquisition of the entire time–resolved fluorescence spectra. The temporal resolution of the up–conversion equipment is about 250 fs, whereas the spectral resolution is 1 nm. Ultrafast spectroscopic data were fitted by Global Analysis using Surface Explorer and Glotaran Softwares.

II. Supplementary Tables and Figures

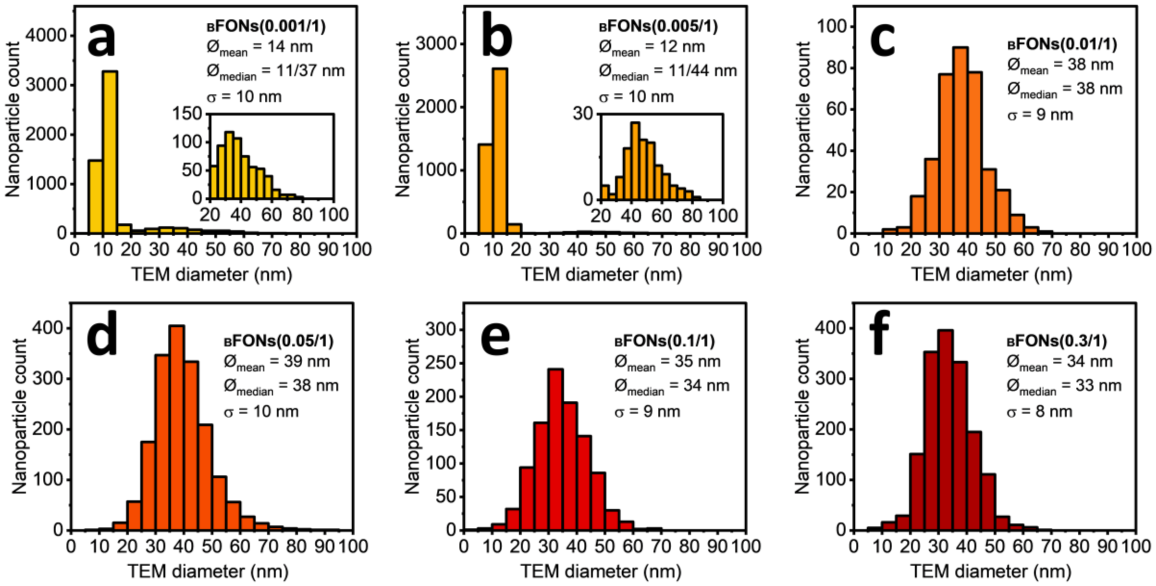

Figure S1. TEM size distributions of BFONs. a) BFONs(0.001/1), b) BFONs(0.005/1), c) BFONs(0.01/1), d) BFONs(0.05/1), e) BFONs(0.1/1), f) BFONs(0.3/1).

Table S1. Median dry diameters ($\varnothing^{TEM}$) and hydrodynamic diameters ($\varnothing^{DLS}$) of BFONs.

Nanoparticles	$\varnothing^{TEM}{}_{median}$ a) ± σ [nm]	$\varnothing^{DLS}$ b) [nm]	PI c)
BFONs(0.3/1)	33 ± 8	105	0.3
BFONs(0.1/1)	34 ± 9	102	0.3
BFONs(0.05/1)	38 ± 10	110	0.2
BFONs(0.01/1)	38 ± 9	92	0.3
BFONs(0.005/1)	11 ± 10 (11 ± 2 / 44 ± 10)*	112	0.3
BFONs(0.001/1)	11 ± 10 (11 ± 2 / 37 ± 12)*	107	0.3

a) Median dry diameter obtained from TEM images ± standard deviation σ $\left(\sigma = \sqrt{\frac{1}{N}\Sigma_{i=1}^{N}(\varnothing_i - \varnothing_{mean})^2}\right)$; *2 populations: overall median diameter (median diameter for each population: $\varnothing_1/\varnothing_2$). b) Mean hydrodynamic diameter measured using dynamic light scattering (DLS). c) Polydispersity index.

Table S2. Photophysical properties of BFONs in water. dFONs for comparison.

Nanoparticles	λ_{abs}^{max} a) [nm]	λ_{em}^{max} b) [nm]	Φ c)	$N^{A}{}_{/1000D}$ d)	EEE e)	$\varepsilon_{BFONs}^{\lambda excD}$ f) [×10^4 M^{-1}cm^{-1}]	N g)	B h) [×10^6 M^{-1}cm^{-1}]
DdFONs(1)	459	586	0.29	-	-	2.2	1500 [1]	9
AdFONs(1)	536	683	0.03	-	-	1.2	2100 [1]	1
BFONs(0.3/1)	464	665	0.08	300	3	1.9	10700	16
BFONs(0.1/1)	460	662	0.20	100	7	2.1	11900	50
BFONs(0.05/1)	461	652	0.25	50	8	2.2	16800	90
BFONs(0.01/1)	458	637	0.33	10	11	2.1	12100	84
BFONs(0.005/1)	460	634	0.35	5	12	2.2	400 (26200)*	3 (203)*
BFONs(0.001/1)	460	611	0.32	1	11	2.1	400 (15600)*	3 (106)*

a) Absorption maximum wavelength. b) Emission maximum wavelength upon excitation of the donor at 445 nm. c) Fluorescence quantum yield upon excitation of the donor at 445 nm. d) Number of acceptors per 1000 donors. e) Environmental Emission Enhancement factor: quantum yield of BFONs divided by that of AdFONs. f) Extinction coefficient of BFONs at the excitation wavelength of the donor (445 nm). g) Theoretical average number of dyes per nanoparticle N (estimated from TEM measurements, assuming a density relative to water of 1.0). 1] Previously published data[1]. h) Theoretical mean brightness per nanoparticle (calculated as the product of the extinction coefficient $\varepsilon_{BFONs}^{\lambda excD}$ at the excitation wavelength 445 nm and the associated fluorescence quantum yield Φ, multiplied by the number of dyes per nanoparticle N).* Secondary but minor population of larger diameters.

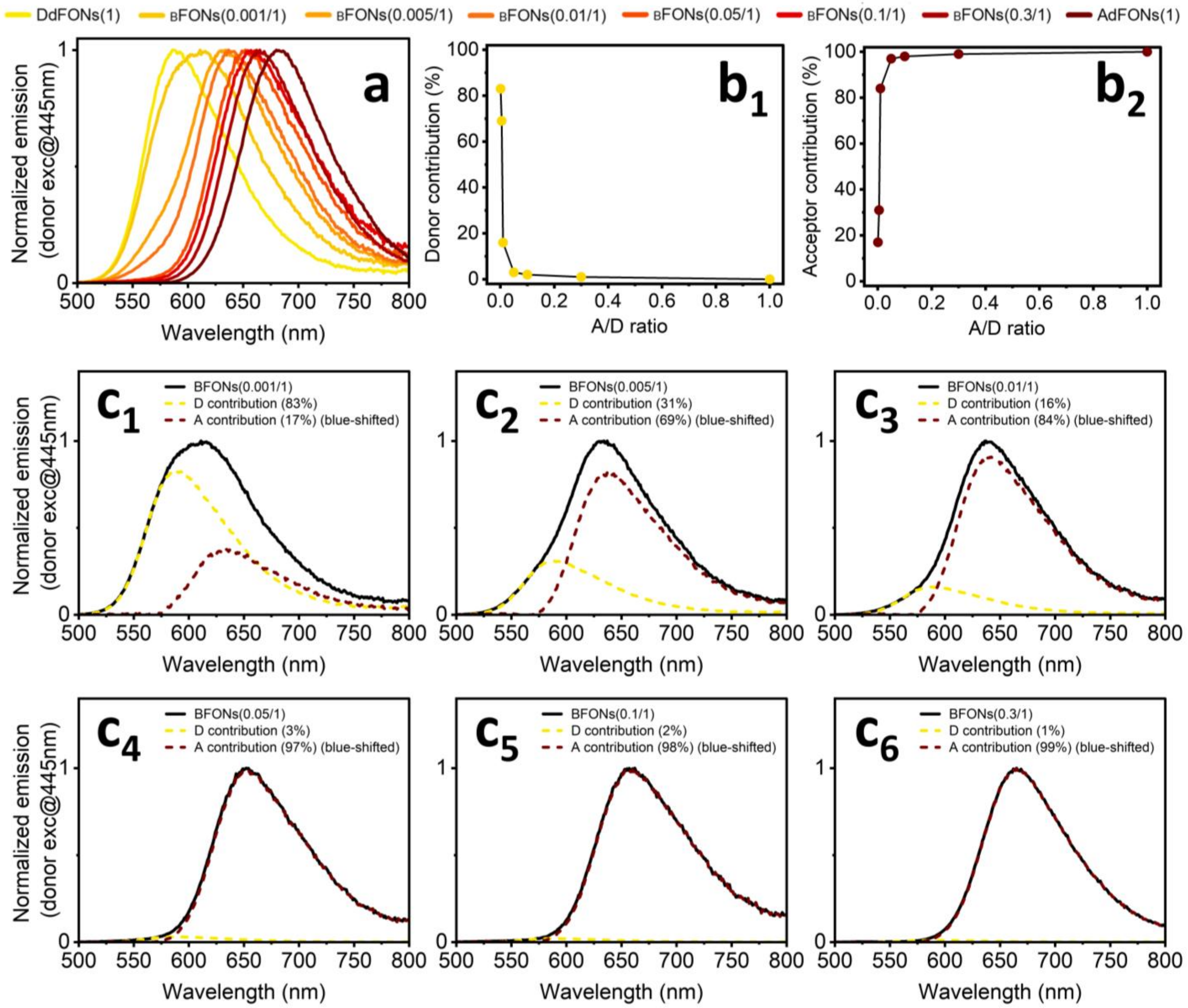

Figure S2. Deconvolution of BFONs emission. a) Normalized emission spectra of dFONs and BFONs suspensions upon donor excitation at 445 nm. b) Donor (b_1) and acceptor (b_2) contributions to the BFONs signal, as a function of the A/D ratio. c) Normalized emission spectra of BFONs (black) upon 445 nm donor excitation, with the donor (yellow) and blue-shifted acceptor (brown) contributions. c_1) BFONs(0.001/1), c_2) BFONs(0.005/1), c_3) BFONs(0.01/1), c_4) BFONs(0.05/1), c_5) BFONs(0.1/1), c_6) BFONs(0.3/1).

Table S3. Emission characteristics of the D and A contributions in BFONs from deconvolution.

Nanoparticles	Donor: Contribution to total [a)] [%]	Donor: Emission intensity [b)] [a.u.]	Donor: FRET efficiency [c)] [%]	Acceptor: Contribution to total [d)] [%]	Acceptor: Emission intensity [e)] [a.u.]	Acceptor: Emission wavelength [f)] [nm]
DdFONs(1)	100	1	-	-	-	-
AdFONs(1)	-	-	-	100	0.02	683
BFONs(0.3/1)	1	0.003	99.7	99	0.29	666
BFONs(0.1/1)	2	0.01	99.0	98	0.47	660
BFONs(0.05/1)	3	0.02	98.0	97	0.66	654
BFONs(0.01/1)	16	0.13	87.0	84	0.76	642
BFONs(0.005/1)	31	0.24	76.0	69	0.68	639
BFONs(0.001/1)	83	0.57	43.0	17	0.29	634

[a)] Donor contribution to the BFONs emission. [b)] Donor emission intensity in BFONs, normalized by the donor emission intensity in DdFONs(1). [c)] FRET efficiency calculated from donor emission intensities. [d)] Acceptor contribution to the BFONs emission. [e)] Acceptor emission intensity in BFONs, normalized by the donor emission intensity in DdFONs(1). [f)] Emission maximum of the acceptor contribution.

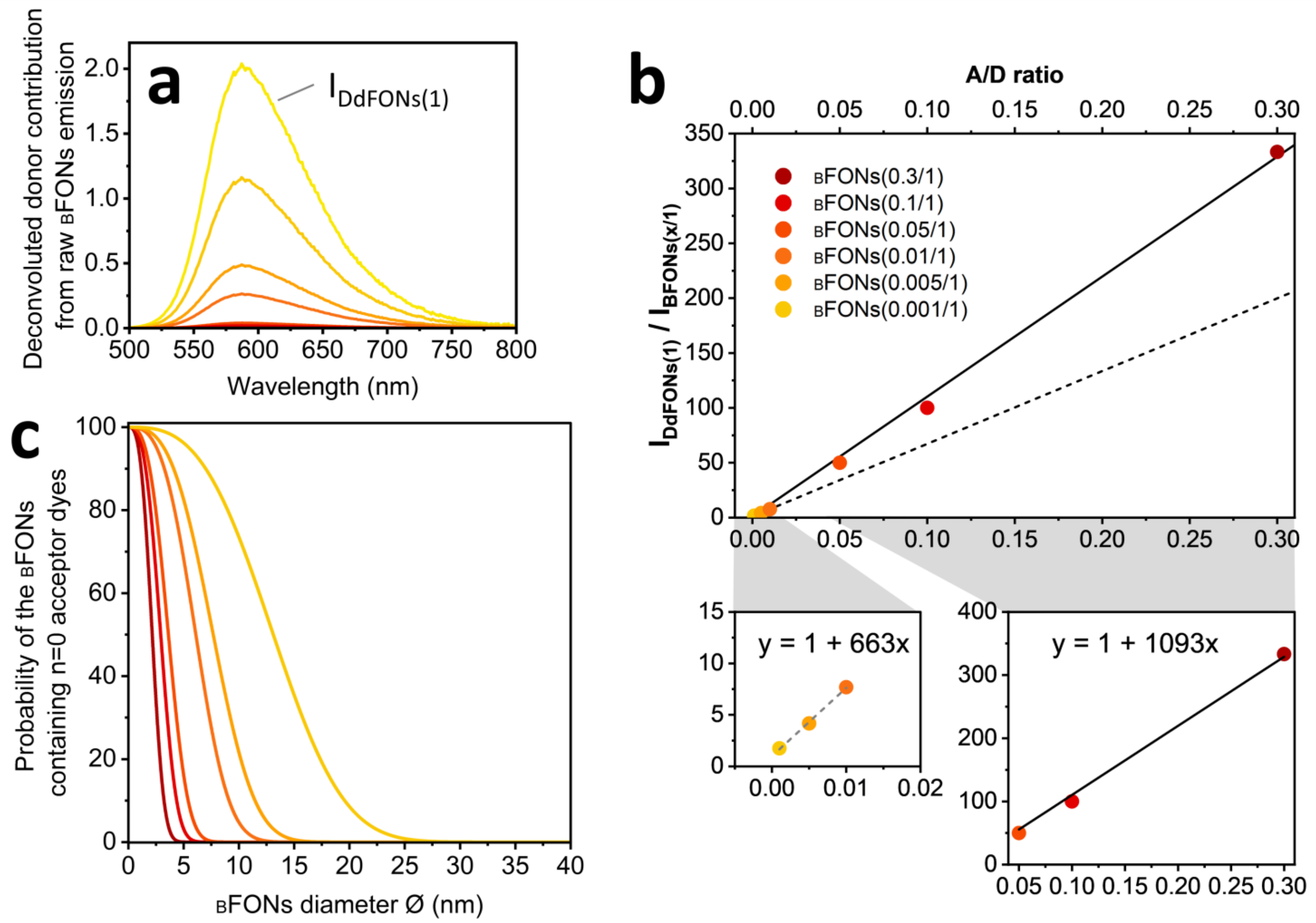

Figure S3. Donor emission contribution in ʙFONs. a) Donor emission contribution, obtained from the deconvolution of the raw emission spectra of ʙFONs upon donor excitation at 445 nm. b) Donor emission quenching as a function of ʙFONs A/D ratio. The lines represent Stern-Volmer plots. Dotted line: low A/D regime, fitted by K_{SV}=663 (one acceptor roughly quenches 663 donors). Solid line: high A/D regime, fitted by K_{SV}=1093 (one acceptor roughly quenches 1093 donors). c) Simulated probability of ʙFONs (with various A/D ratios) containing n=0 acceptor dyes, as a function of their diameter, based on a Poisson distribution model.

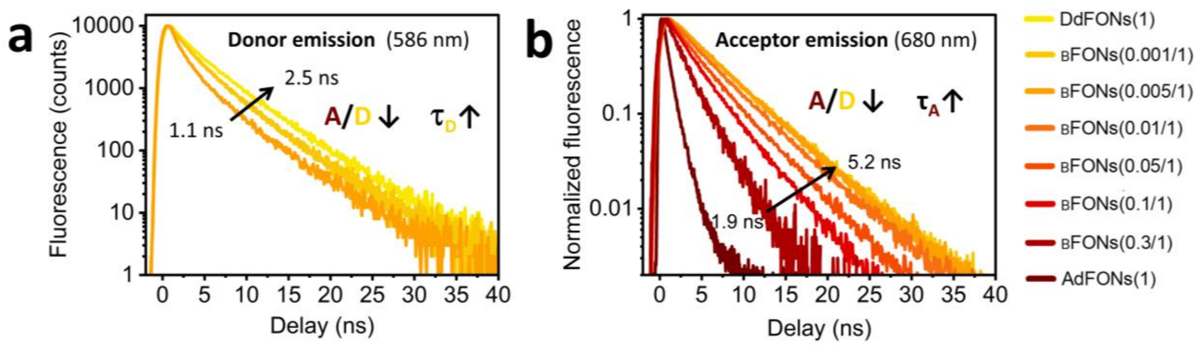

Figure S4. Fluorescence decays upon donor excitation. a) Fluorescence decay of the donor emission in dFONs and ʙFONs at 586 nm upon excitation at 445 nm. b) Fluorescence decay of the acceptor emission in dFONs and ʙFONs at 680 nm upon excitation at 445 nm.

Table S4. Fluorescence lifetimes of dyes D and A as FONs subunits upon excitation at 455 nm.

Nanoparticles	D (em 586 nm)			A (em 680 nm)		
	τ^{int}_{avgD} [a] [ns]	τ^{amp}_{avgD} [b] [ns]	χ^2_D [c]	τ^{int}_{avgA} [d] [ns]	τ^{amp}_{avgA} [e] [ns]	χ^2_A [f]
DdFONs(1)	3.8	2.5	1.09	4.2	3.6	1.02
AdFONs(1)	-	-	-	1.0	0.5	1.24
BFONs(0.3/1)	UD[1)]	UD[1)]	UD[1)]	2.3	1.9	1.00
BFONs(0.1/1)	UD[1)]	UD[1)]	UD[1)]	3.4	1.8	1.07
BFONs(0.05/1)	UD[1)]	UD[1)]	UD[1)]	4.1	2.5	0.97
BFONs(0.01/1)	1.7	0.6	0.95	4.9	4.5	0.97
BFONs(0.005/1)	2.4	1.1	1.09	5.3	5.1	1.12
BFONs(0.001/1)	3.2	2.0	1.12	5.4	5.2	1.18

UD[1)] = Undetectable: the fluorescence signal was too weak to be detected (complete quenching of the fluorescence of D). [a)] Intensity-averaged fluorescence lifetime: detection of D emission at 586 nm upon excitation at 455 nm. [b)] Amplitude-averaged fluorescence lifetime: detection of D emission at 586 nm upon excitation at 455 nm. [c)] Goodness of fit (ideal value: χ^2 =1). [d)] Intensity-averaged fluorescence lifetime: detection of A emission at 680 nm upon excitation at 455 nm. [e)] Amplitude-averaged fluorescence lifetime: detection of A emission at 680 nm upon excitation at 455 nm. [f)] Goodness of fit (ideal value: χ^2 =1).

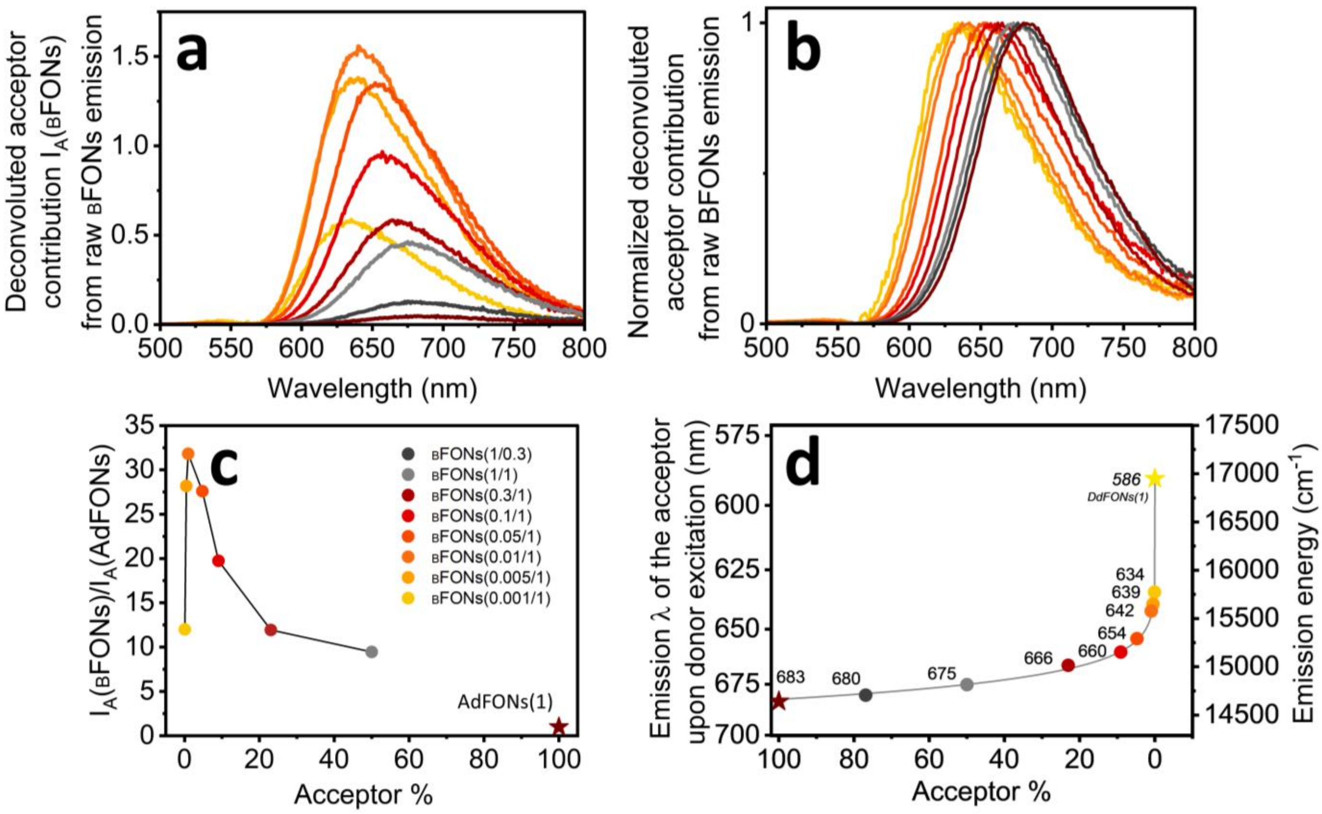

Figure S5. Acceptor emission contribution in BFONs. a) Acceptor emission contribution, obtained from the deconvolution of the raw emission spectra of BFONs upon donor excitation at 445 nm. b) Normalized emission spectra of BFONs acceptor contribution. c) Acceptor emission intensity of BFONs, normalized by the emission intensity of AdFONs, as a function A/D ratio. d) Maximum emission wavelength of the acceptor contribution of BFONs, as a function of acceptor content. Left axis: Emission wavelength. Right axis: Associated emission energy.

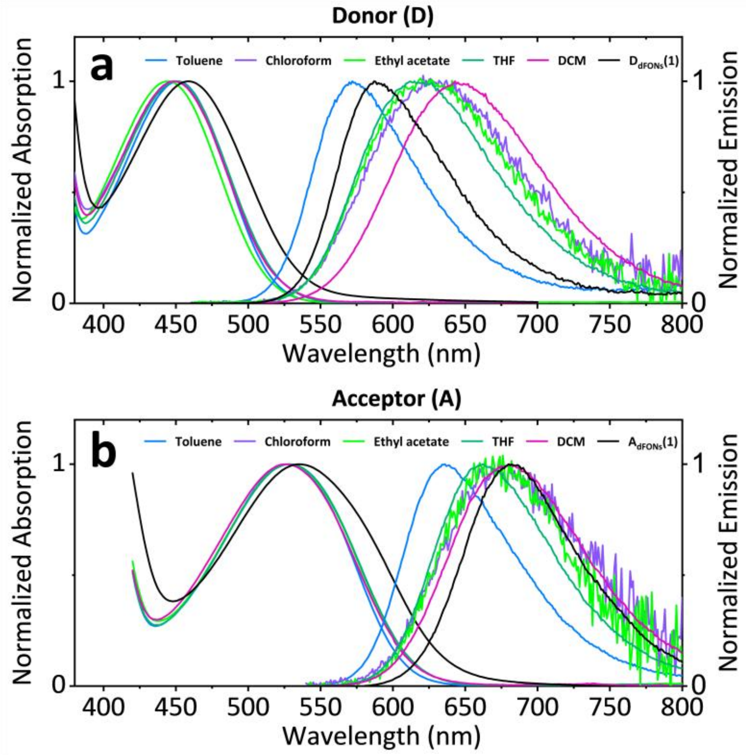

Figure S6 Absorption and emission spectra of a) dye D and b) dye A in toluene, chloroform, ethyl acetate, tetrahydrofuran, dichloromethane and water (dFONs).

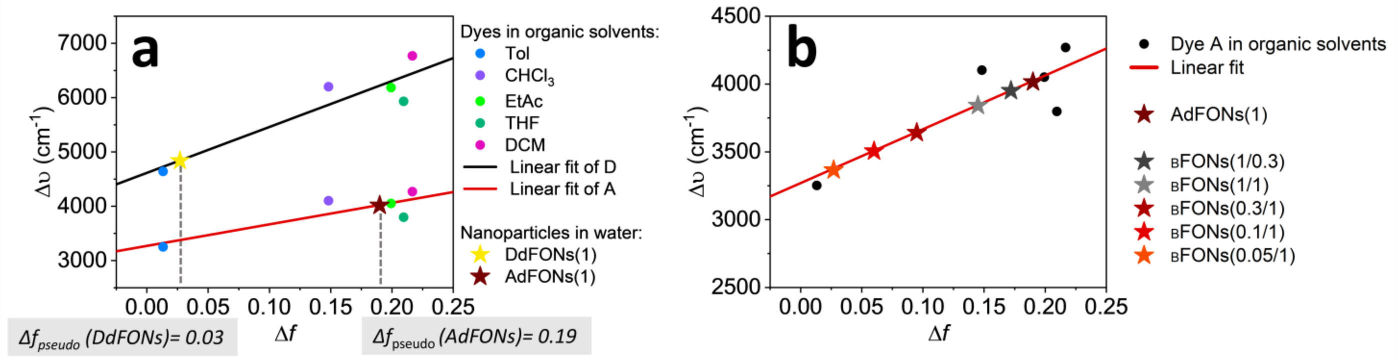

Figure S7. a) Lippert-Mataga plots of D and A, constructed through a linear fit from the Stokes Shift values of the dyes in toluene (Tol), chloroform ($CHCl_3$), ethyl acetate (EtAc), tetrahydrofuran (THF), and dichloromethane (DCM). The Stokes Shift of DdFONs(1) and AdFONs(1) were added to the plot, and the Δf manually adjusted in order to estimate the orientational polarizability of the D bulk material in DdFONs and of the A bulk material in AdFONs, resulting in respectively Δf_{pseudo}(DdFONs)=0.03 and Δf_{pseudo} (AdFONs)=0.19. b) Lippert-Mataga plot of A, on which the Stokes shifts of various BFONs were added, and the Δf manually adjusted in order to estimate the orientational polarizability Δf of the BFONs bulk material (likely a statistical mixture of dyes A and D), resulting in Δf_{pseudo}(AdFONs)>Δf_{pseudo} (BFONs)>Δf_{pseudo} (DdFONs) for BFONs(1/0.3) to BFONs(0.05/1). BFONs with a lower A/D ratio could not be added to the plot due to their very small Stokes shifts.

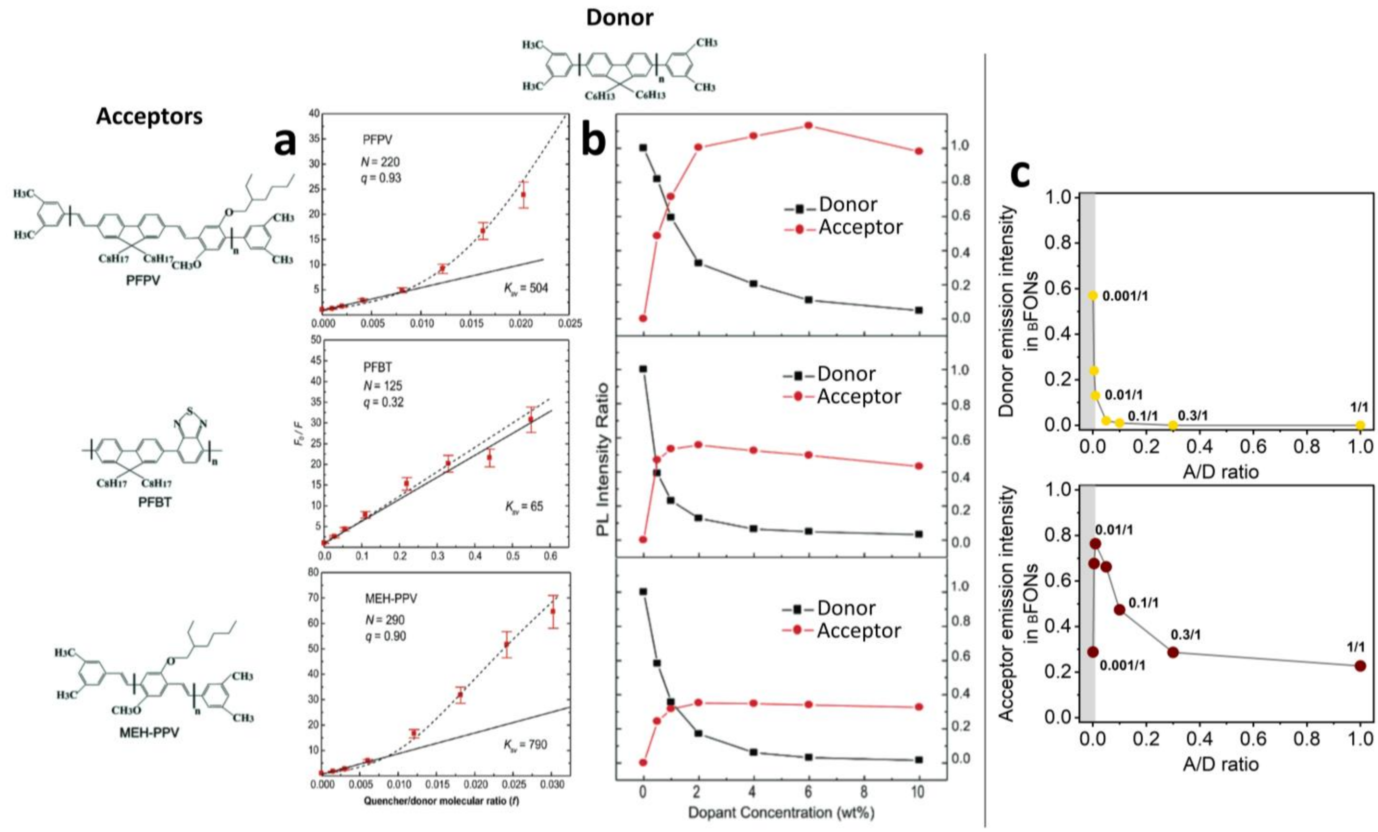

Figure S8. Comparison with literature. (Panels a and b adapted with permission from.[6]) a) Fluorescence quenching of donor versus molar fraction of acceptors in blended conjugated polymer nanoparticles. Solid line: linear Stern-Volmer plots in the low concentration range. b) Donor (black) and acceptor (red) emission intensities of blended conjugated polymer nanoparticles as a function of the molar fraction of acceptors (normalized by the emission intensity of pure donor particles). c) Donor (top) and acceptor (bottom) emission intensity of BFONs as a function of the A/D ratio (normalized by the emission intensity of DdFONs(1)). The abrupt change in the grey region is attributed to a high likelihood of forming DdFONs in this low A/D ratio domain.

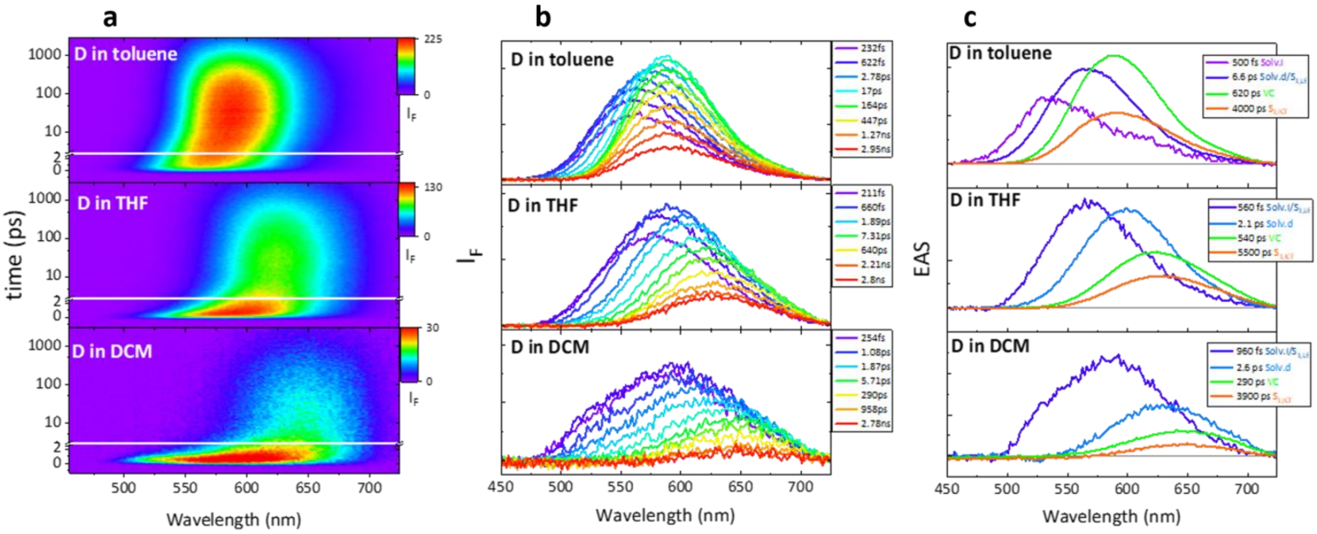

Figure S9. Femtosecond Broadband Fluorescence Up Conversion spectroscopy of D in toluene, tetrahydrofuran (THF) and dichloromethane (DCM): a) 3D data matrices, b) time-resolved emission spectra and c) Evolution Associated Spectra obtained from Global Analysis.

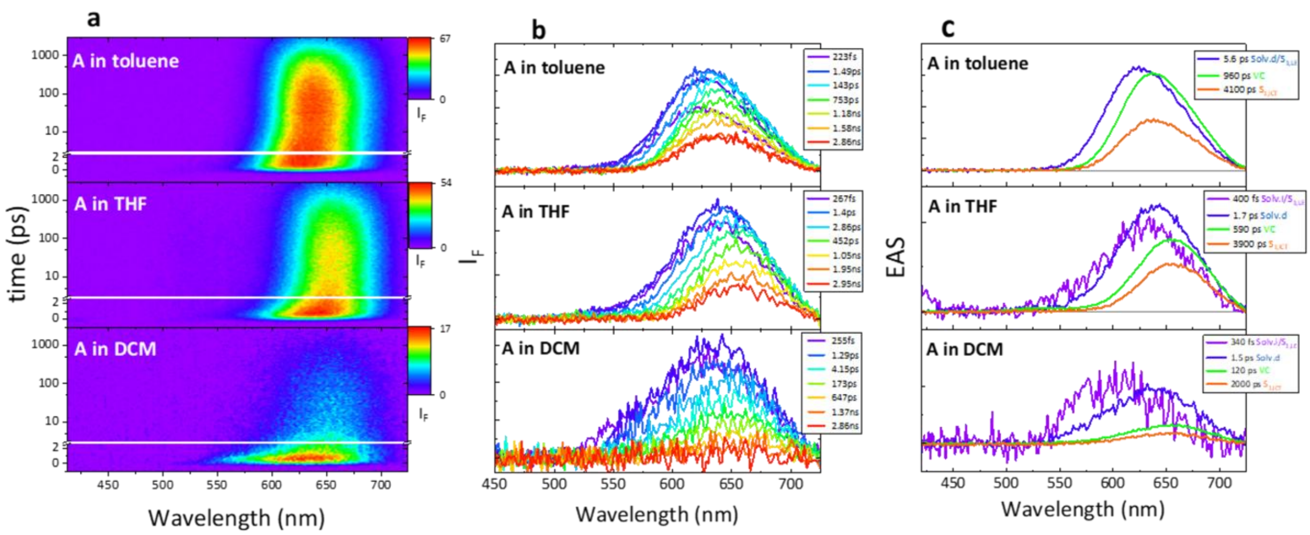

Figure S10. Femtosecond Broadband Fluorescence Up Conversion spectroscopy of A in toluene, tetrahydrofuran (THF) and dichloromethane (DCM): a) 3D data matrices, b) time-resolved emission spectra and c) Evolution Associated Spectra obtained from Global Analysis.

Table S5. Results of the Global Analysis of the Femtosecond Transient Absorption (TA) and Broadband Fluorescence Up Conversion (FUC) data of D and A in solvents of different polarity: toluene, tetrahydrofuran (THF) and dichloromethane (DCM).

Dye	Solvent	τ_{TA} [ps]	τ_{FUC} [ps]	Assignment
D	Toluene	0.27	0.50	Solv.i
		5.2	6.6	Solv.d / $S_{1,LE}$
		430	620	VC
		4000	4000	$S_{1,ICT}$
	THF	0.31	0.56	Solv.i / $S_{1,LE}$
		2.0	2.1	Solv.d
		390	540	VC
		5500	5500	$S_{1,ICT}$
	DCM	0.22	0.96	Solv.i / $S_{1,LE}$
		1.2	2.6	Solv.d
		160	290	VC
		3900	3900	$S_{1,ICT}$
A	Toluene	4.9	5.6	Solv.d / $S_{1,LE}$
		660	960	VC
		4100	4100	$S_{1,ICT}$
	THF		0.40	Solv.i
		2.9	1.7	Solv.d /$S_{1,LE}$
		890	590	VC
		3900	3900	$S_{1,ICT}$
	DCM		0.34	Solv.i
		2.4	1.5	Solv.d /$S_{1,LE}$
		250	120	VC
		2000	2000	$S_{1,ICT}$

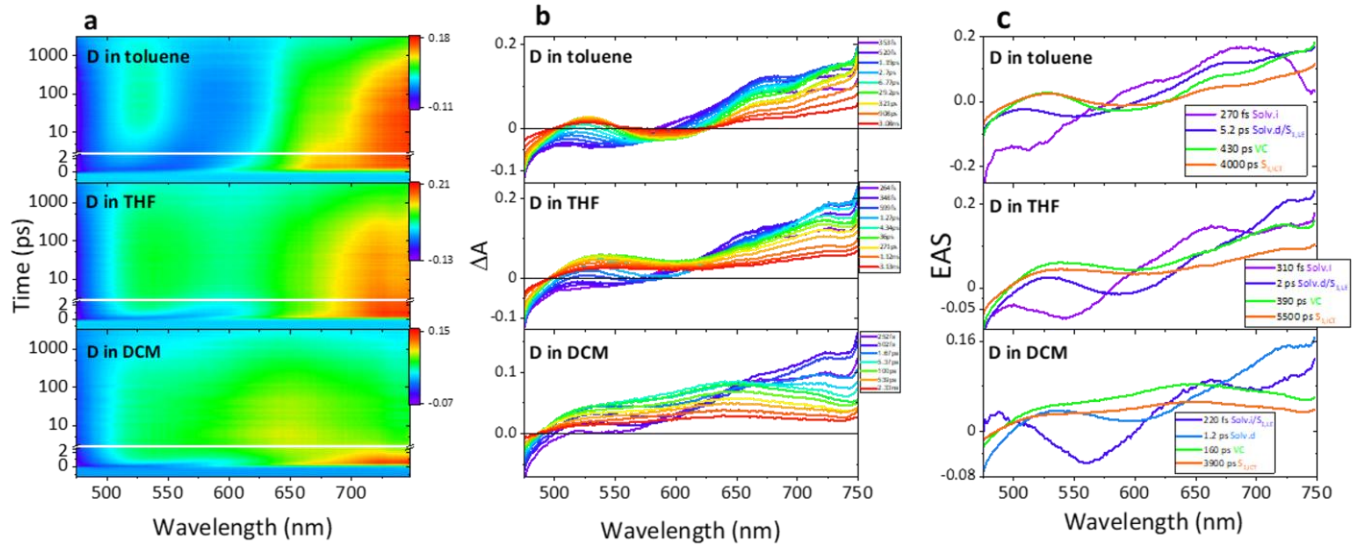

Figure S11. Femtosecond Transient Absorption spectroscopy of D in toluene, tetrahydrofuran (THF) and dichloromethane (DCM): a) 3D data matrices, b) time-resolved absorption spectra and c) Evolution Associated Spectra obtained from Global Analysis.

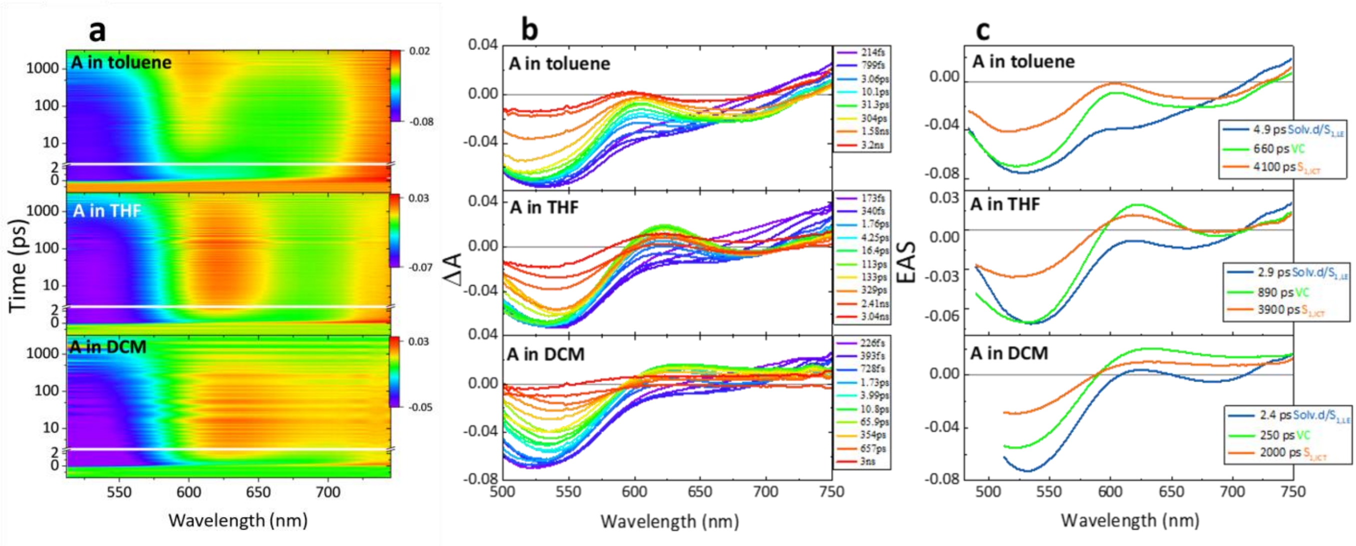

Figure S12. Femtosecond Transient Absorption spectroscopy of A in toluene, tetrahydrofuran (THF) and dichloromethane (DCM): a) 3D data matrices, b) time-resolved absorption spectra and c) Evolution Associated Spectra obtained from Global Analysis.

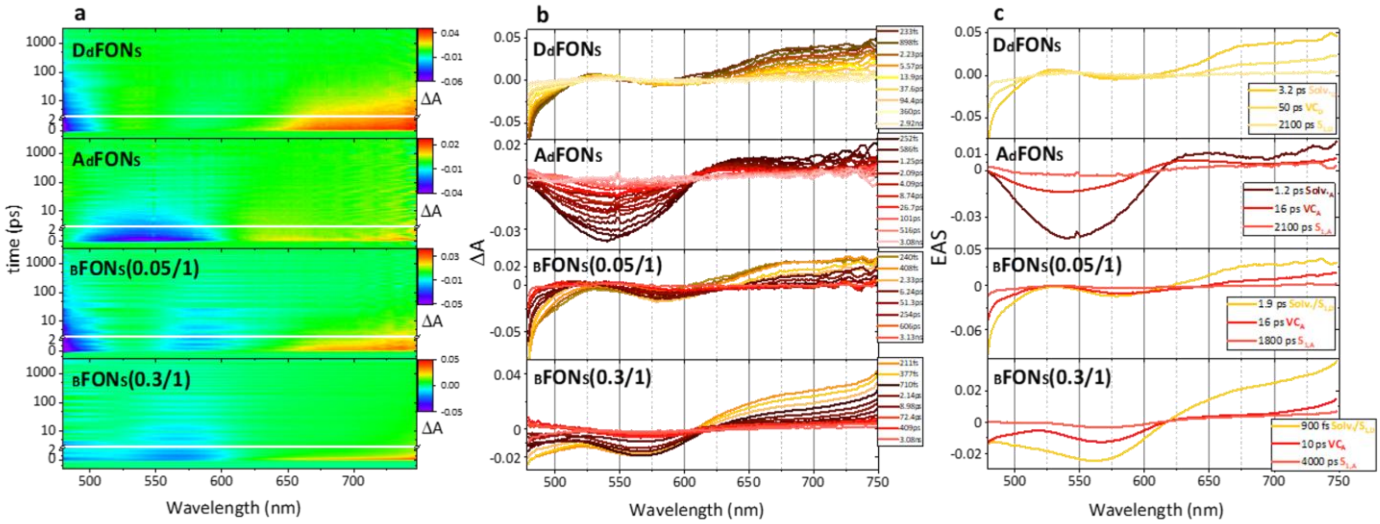

Figure S13. Femtosecond Transient Absorption spectroscopy of aqueous suspensions of DdFONs, AdFONs, BFONs(0.05/1) and BFONs(0.3/1): a) 3D data matrices, b) time-resolved absorption spectra and c) Evolution Associated Spectra obtained from Global Analysis.

Table S6. Results of the Global Analysis of the Femtosecond Transient Absorption (TA) and Broadband Fluorescence Up Conversion (FUC) data of aqueous suspensions of DdFONs, AdFONs, BFONs(0.05/1) and BFONs(0.3/1).

Nanoparticles	τ_{TA} [ps]	τ_{FUC} [ps]	Assignment
D_{dFONs}(1)	**3.2**	**2.2**	**Solv.$_D$**
	50	**36**	**VC$_D$**
	2100	**1550**	**$S_{1,D}$**
A_{dFONs}(1)	**1.2**	**2.0**	**Solv.$_A$**
	16	**18**	**VC$_A$**
	2100	**2000**	**$S_{1,A}$**
BFONs(0.05/1)	**1.9**	**2.2**	**Solv.$_D$ / $S_{1,D}$**
	16	**38**	**VC$_A$**
	1800	**2000**	**$S_{1,A}$**
BFONs(0.3/1)	**0.90**	**0.97**	**Solv.$_D$ / $S_{1,D}$**
	10	**11**	**VC$_A$**
	4000	**2000**	**$S_{1,A}$**

References

1 P. Pagano, M. Rosendale, J. Daniel, J.-B. Verlhac and M. Blanchard-Desce, *J. Phys. Chem. C*, 2021, **125**, 25695–25705.

2 J. Baumann and M. D. Fayer, *The Journal of Chemical Physics*, 1986, **85**, 4087–4107.

3 Y. Rout, C. Montanari, E. Pasciucco, R. Misra and B. Carlotti, *J. Am. Chem. Soc.*, 2021, **143**, 9933–9943.

4 M. Alebardi, C. Munzone, E. Sorbelli, A. Grasso, L. Mencaroni, F. Elisei, C. G. Fortuna, A. Spalletti, C. Bonaccorso and B. Carlotti, *Advanced Functional Materials*, 2024, **34**, 2403706.

5 L. Mencaroni, B. Carlotti, F. Elisei, A. Marrocchi and A. Spalletti, *Chem. Sci.*, 2022, **13**, 2071–2078.

6 C. Wu, H. Peng, Y. Jiang and J. McNeill, *J. Phys. Chem. B*, 2006, **110**, 14148–14154.